Journal of Colloid and Interface Science 445 (2015) 1–8

Contents lists available at ScienceDirect

Journal of Colloid and Interface Science

www.elsevier.com/locate/jcis

Rapid adsorption of 2,4-dichlorophenoxyacetic acid by iron oxide nanoparticles-doped carboxylic ordered mesoporous carbon

Lin Tang *, Sheng Zhang, Guang-Ming Zeng *, Yi Zhang, Gui-De Yang, Jun Chen, Jing-Jing Wang, Jia-Jia Wang, Yao-Yu Zhou, Yao-Cheng Deng

College of Environmental Science and Engineering, Hunan University, Changsha 410082, PR China
Key Laboratory of Environmental Biology and Pollution Control (Hunan University), Ministry of Education, Changsha 410082, PR China

GRAPHICAL ABSTRACT

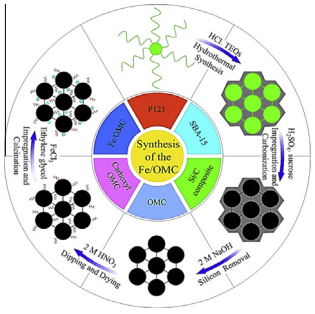

ARTICLE INFO

Article history:
Received 24 August 2014
Accepted 22 December 2014
Available online 3 January 2015

Keywords:
Ordered mesoporous carbon
Iron oxide nanoparticles
2,4-Dichlorophenoxyacetic acid
Adsorption

ABSTRACT

The ordered mesoporous carbon composite functionalized with carboxylate groups and iron oxide nanoparticles (Fe/OMC) was successfully prepared and used to adsorb 2,4-dichlorophenoxyacetic acid (2,4-D) from wastewater. The resultant adsorbent possessed high degree of order, large specific surface area and pore volume, and good magnetic properties. The increase in initial pollutant concentration and contact time would make the adsorption capacity increase, but the pH and temperature are inversely proportional to 2,4-D uptake. The equilibrium of adsorption was reached within 120 min, and the equilibrated adsorption capacity increased from 99.38 to 310.78 mg/g with the increase of initial concentration of 2,4-D from 100 to 500 mg/L. Notablely, the adsorption capacity reached 97% of the maximum within the first 5 min. The kinetics and isotherm study showed that the pseudo-second-order kinetic and Langmuir isotherm models could well fit the adsorption data. These results indicate that Fe/OMC has a good potential for the rapid adsorption of 2,4-D and prevention of its further diffusion.

1. Introduction

2,4-Dichlorophenoxyacetic acid (2,4-D) is a typical chlorinated aromatic compound herbicide, which was firstly synthesized and commercially marketed in USA in the early 1940s [1]. The structural diagram of 2,4-D is shown in Fig. 1. It is commonly used for the control of broad-leafed weeds in gardens and farms [2,3]. 2,4-D is a commonly preferred herbicide because of its low cost and good selectivity [4,5], and can be found in surface and ground water all over the world. The World Health Organization identifies 2,4-D as moderately toxic (Class II) to human beings and animals and recommends 70 μg/L as the maximum permissible concentration in drinking water [6]. When people are exposed to 2,4-D for a long time, it would result in moderate and serious skin

* Corresponding authors.
E-mail addresses: tanglin@hnu.edu.cn (L. Tang), zgming@hnu.edu.cn (G.-M. Zeng).

http://dx.doi.org/10.1016/j.jcis.2014.12.074
0021-9797/

and eye irritation, even produce potentially carcinogenic risk [2]. Hence, it is extremely urgent to remove 2,4-D from the environment. Many methods have been used to remove 2,4-D from water. For example, photocatalytic degradation [7], combined microwave-assisted degradation and UV irradiation [8], biological degradation [9], electrocatalytic dechlorination [10,11], electro-biological degradation [12], chemical oxidation with hydrogen peroxide [13], and adsorption [14,15].

Among these technologies, the adsorption approach is the most commonly used technique to remove toxic substances from wastewater due to its low cost, ease of operation, insensitivity to toxic pollutants, flexibility and simplicity of design [6,16]. Among all the adsorbing materials (such as clays [17], porous polymeric adsorbents [18], resin [19], activated carbon [20], Zn–Al–Zr layered double hydroxide [21], ordered mesoporous carbon [22], etc.), ordered mesoporous carbon (OMC) is an excellent candidate because of its highly-enlarged surface area and pore volume, chemical inertness and thermal stability [23–27]. However, it has some weaknesses relating with its inherent properties. On one hand, its hydrophilicity is very poor, which results in bad dispersity in aqueous solution. On the other hand, it is likely to cause secondary pollution because of its difficult reclaimation. Therefore, it is quite necessary to improve the properties of OMCs by taking some measures. A previous study indicated nitric acid oxidation can introduce carboxyl groups into the carbon material and further change its surface hydrophobic/hydrophilic balance [28]. Furthermore, carboxyl groups of the OMC can provide weak acid sites, which is beneficial to the immobilization of organic pesticide [28]. Meanwhile, the introduction of magnetic components into OMC can accelerate the separation and recovery of the materials by external magnetic fields [29], and prevent secondary pollution.

In this study, an iron oxide nanoparticles-doped ordered mesoporous carbon functionalized with carboxylate groups (Fe/OMC) was successfully prepared by impregnation and then calcination. The functionalized mesoporous carbon was characterized by a series of physical-chemical techniques, and the excellent hydrophilicity and magnetic separability could be confirmed. The prepared Fe/OMC adsorbent was used to remove 2,4-D from aqueous solution. The effects of contact time, pH, initial 2,4-D concentration, and reusability of the materials for 2,4-D adsorption were also investigated. Kinetics, sorption isotherm and thermodynamics were used to expound the relevant adsorption mechanism.

2. Experimental section

2.1. Materials

2,4-D (the purity of 98%) and Pluronic copolymer P123 ($EO_{20}PO_{70}EO_{20}$, EO = ethylene oxide, PO = propylene oxide) were supplied by Sigma–Aldrich Corp. Other chemical reagents were of analytical reagent grade and were purchased from Shanghai Chemical Corp. The water used in laboratory was high-purity water (18.25 MΩ cm^{-1}) from a Millipore Milli-Q water purification system.

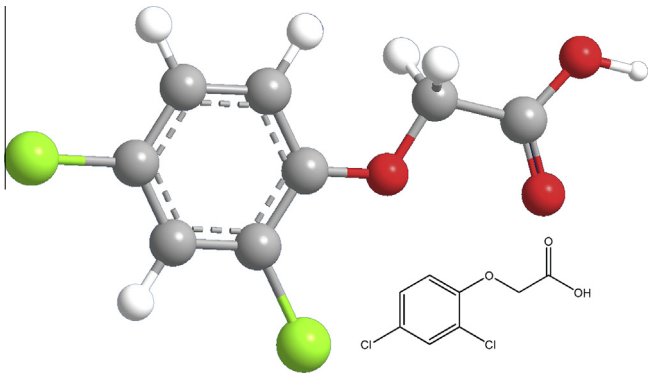

Fig. 1. Structural diagram of 2,4-D.

2.2. Preparation of adsorbent

2.2.1. Synthesis of SBA-15

Mesoporous SBA-15 was prepared according to the process described by Zhao et al. [30]. 8.0 g of P123 was dissolved in a solution containing 270 mL water and 42 mL HCl at 35 °C in a triangle flask, and the solution was continuously stirred. After P123 was completely dissolved, 17 g tetraethyl orthosilicate was dropwise added to the above solution, and the mixture was sequentially stirred for 20 h. Then the mixture was aged in drying oven at 140 °C for 24 h by digestion tank. Subsequently, the product was washed with high-purity water until the pH was close to 7, and dried at 60 °C for 20 h. To remove P123 template, the resultant solid was finally calcined in static air at 550 °C for 4 h with a heating rate of 1 °C min^{-1}.

2.2.2. Synthesis of ordered mesoporous carbon

Ordered mesoporous carbon was synthesized by using sucrose as carbon source and SBA-15 as hard template according to a previous publication [31]. The solution containing 1.25 g sucrose, 0.145 g H_2SO_4 and 5 mL H_2O was dropwise added to 1 g SBA-15 with the mixture being stirred occasionally at the same time. The resulting product was heated in an oven at 100 °C for 6 h and then at 160 °C for another 6 h. The polymer composites were then heat-treated in nitrogen flow at 900 °C for 2 h with a heating rate of 2 °C min^{-1}. 2 M NaOH aqueous solutions were used to remove SBA-15 template at 90 °C for 1 h, which was repeated. The silica-free ordered mesoporous carbon was obtained and thoroughly washed with high-purity water until neutral, and dried in oven at 60 °C for 24 h.

2.2.3. Synthesis of the functionalized ordered mesoporous carbon

The functionalized ordered mesoporous carbon was synthesized according to previous reports [29,32]. Carboxyl groups were grafted to ordered mesoporous carbon by dipping the material in 2 M HNO_3 aqueous solution at 80 °C for 1.5 h. Then the powder was filtered and washed with high-purity water and dried at 60 °C. After that, Iron oxide nanoparticles were deposited on the pores of carboxyl ordered mesoporous carbon. 100 mg of carboxyl-ordered mesoporous carbon was added to a solution containing 40 mL of ethanol and 120 mg of anhydrous ferric chloride. The resulting solution was stirred at 60 °C for 1 h. To remove the remaining iron, the obtained dry powder was washed with ethanol several times, until the filtrate was clear. The washed carbon was dried in vacuum at 30 °C for 12 h. Subsequently, the obtained carbon powder was impregnated with about 1 g ethylene glycol, and the residual ethylene glycol was blotted up carefully with filter paper. Eventually, the carbon powder was heated to 510 °C with 2 °C min^{-1} rate under nitrogen atmosphere for 1 h to obtain magnetic ordered mesoporous carbon denoted by Fe/OMC. The detailed synthesis routes of Fe/OMC are shown in Fig. 2.

2.3. Materials characterization

Transmission electron microscopy (TEM) was carried out in a JEOL-1230 electron microscope operated at an acceleration voltage of 100 KeV. Nitrogen physisorption isotherms were carried out at −196 °C on a Micromeritics 2020 analyzer. The surface area was calculated with the Brunauer, Emmet and Teller (BET) equation. The pore size distribution curves and total pore volume were

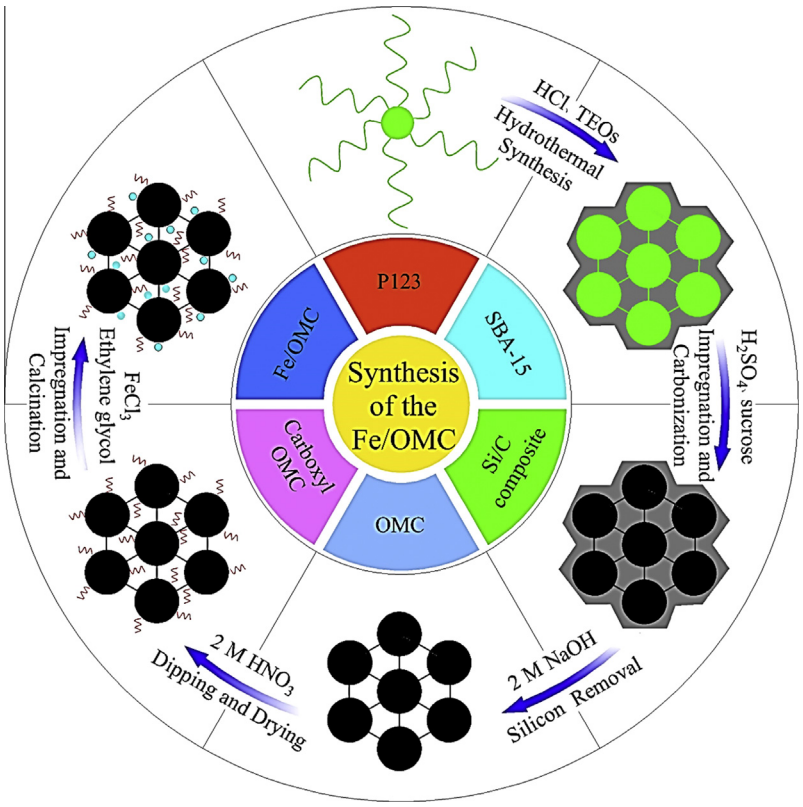

Fig. 2. Synthesis process of Fe/OMC.

derived respectively from the adsorption branches of isotherms and desorption branches of isotherms by using the Barett–Joyner–Halenda (BJH) method. X-ray diffraction (XRD) analysis was performed on a SIEMENSD 5005 diffractometer with Cu Kα X-ray source, working at 30 kV and 15 mA. The magnetization of the adsorbents was measured by a vibrating sample magnetometer (VSM). Fourier transform infrared (FTIR) spectra were collected on Nicolet NEXUS 670 FTIR spectrometer using the standard KBr disk method.

2.4. Batch experiments

All batch studies were carried out in 50 mL conical flask containing 10 mg Fe/OMC and 10 mL 2,4-D solution. The difference adsorption conditions such as, initial concentration (50–500 mg/L), pH of the solution (3–11), contact time (5–420 min) and temperatures (30–50 °C) were investigated in Water-bathing Constant Temperature Vibrator with an agitation speed of 120 rpm. The equilibrium and kinetic experiments were carried out at pH 3. After each experimental, the residual concentration of 2,4-D was measured using a double beam UV–Vis spectrophotometer (Shimadzu, UV-2550, Japan) at wavelength of 284 nm. The average values of all the experiments were collected by three parallel tests. The amount of adsorption (q_t) at time t and the percentage of removal (R_r) were calculated using Eqs. (1) and (2), respectively. Formula follows.

$$q_t = \frac{(C_0 - C_t) \times V}{W} \quad (1)$$

$$R_r(\%) = \frac{(C_0 - C_t)}{C_0} \times 100\% \quad (2)$$

where C_0 and C_t (mg/L) represent the solution concentrations of 2,4-D at the initial and time t, respectively; W (mg) is the mass of dry adsorbent; V (mL) is the volume of 2,4-D solution; q_t is the amount of adsorbed 2,4-D at time t; R_r is the percentage of removal for 2,4-D.

3. Results and discussion

3.1. Characterization of materials

Fig. 3 shows the transmission electron microscopy (TEM) images of the pure OMC and Fe/OMC. The stripe-like structures were clearly seen for the two materials. This indicated that both materials possess a mesoporous structure. However, as shown in Fig. 3, the definition of stripe-like structures of OMC is obviously higher than Fe/OMC. It means that the degree of order of Fe/OMC was inferior to OMC, which was related to nitric acid oxidation treatment and introduction of Fe_3O_4 nanoparticles. Firstly, nitric acid oxidation treatment was used to graft carboxyl groups to OMC for changing the OMC surface hydrophobic/hydrophilic balance and improving the wettability of the mesoporous carbon. However, nitric acid is a strong oxidizing agent. According to the study by Wu et al.'s work [28], somewhat excessive oxidization of carbon in pore walls by nitric acid was inevitable, which would result in partial collapse of pore canals and reduce the degree of the order of OMC. Secondly, the Fe^{3+} ions could be captured by chemical complexation to the carboxyl groups of OMC, which was of benefit to the in situ nucleation of nanoparticles. But carbon atoms in the pore wall might participate in the reduction of Fe^{3+}, leading to reduction of degree of the order. In Fig. 3b, the black dots that represent the Fe_3O_4 nanoparticles were distributed evenly over the OMC.

The nitrogen adsorption–desorption isotherms of OMC and Fe/OMC are shown in Fig. 4a which belong to type IV isotherm with a H1 hysteresis loop. Hysteresis loop of Fe/OMC is located at P/P_0 between 0.6 and 0.8, indicating that the two carbon materials had uniform mesoporous structures. The pore size distributions

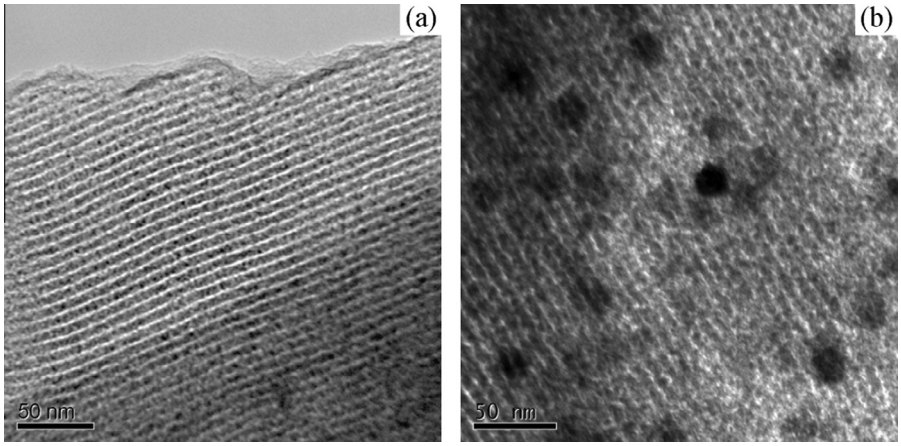

Fig. 3. TEM images of OMC (a) and Fe/OMC (b).

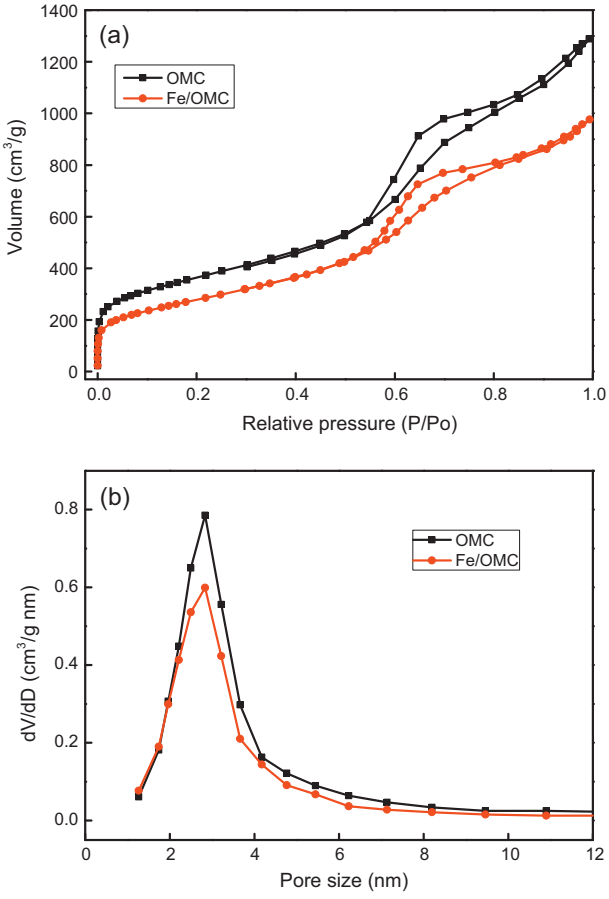

Fig. 4. Nitrogen adsorption–desorption isotherms (a) and pore size distribution (b) of OMC and Fe/OMC.

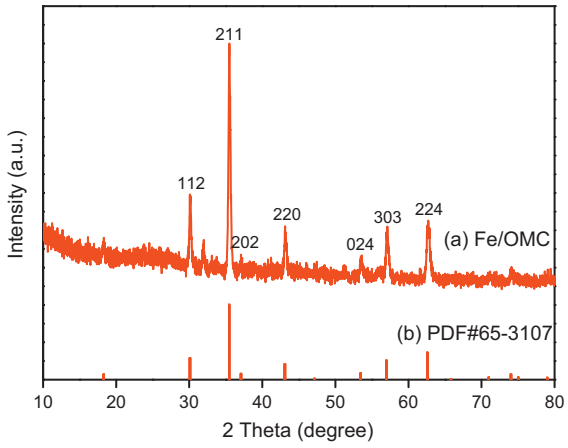

Fig. 5. XRD spectra of Fe/OMC.

of Fe/OMC (Fig. 4b) calculated from the adsorption branch clearly determines the pore size to be mainly in the range of 2–4 nm, and the average pore size of OMC and Fe/OMC are both 2.83 nm. In addition, with the introduction of Fe_3O_4 nanoparticles into carbon materials, the surface area (from 1054.50 to 882.52 m^2/g) and pore volume area (from 1.85 to 1.43 cm^3/g) were decreased. The reason of the decrease might be that the introduction of Fe_3O_4 nanoparticles would occupy or block pore canals.

The high-angle XRD diffractograms (Fig. 5) are used to identify the crystalline phases formed upon modification of OMC, and further indicate the presence of Fe_3O_4 nanoparticles. All the primary diffraction peaks of Fe/OMC at 2θ of 30.1°, 35.5°, 37.1°, 43.1°, 53.6°, 57.1° and 62.7°, corresponding to (112), (211), (202), (220), (024), (303) and (224) reflections, agreed well with the standard orthorhombic phase of Fe_3O_4 (JCPDS card No. 65-3107). These mean that the orthorhombic phase of Fe_3O_4 was dominant in the carbon material.

FTIR spectra of the OMC and Fe/OMC are shown in Fig. 6. The FTIR spectrum of the OMC (Fig. 6a) has only a few weak broad absorption bands, due to the high carbonization of material. Nevertheless, in the FTIR spectrum of Fe/OMC (Fig. 6b), six obvious bands are centered around 573, 1153, 1574, 1730, 3450 cm^{-1} relative to OMC after the oxidative treatment of nitric acid and dipping of Fe_3O_4 nanoparticles. The absorbance band at 1730 cm^{-1} is the C═O stretching vibration in Fe/OMC. The broad peak at 3450 cm^{-1} is attributed to the –OH vibration. The above two bands indicate that the carboxyl group was successfully introduced to the surface of Fe/OMC. COOH is the main form of the carboxyl group existing in acid condition. These weak acid sites of carboxyl group are beneficial to the immobilization of organic pesticide (2,4-D). The characteristic peak at 1574 cm^{-1} corresponds to the symmetric COO^- vibration. COO^- is the main form of existence in alkali condition. When solution pH increases to be alkaline, the electrostatic repulsion between the increasing negative charged COO^- group and 2,4-D will result in the decrease of adsorption amount for 2,4-D. The band at 1153 cm^{-1} might correspond to the C—O—C

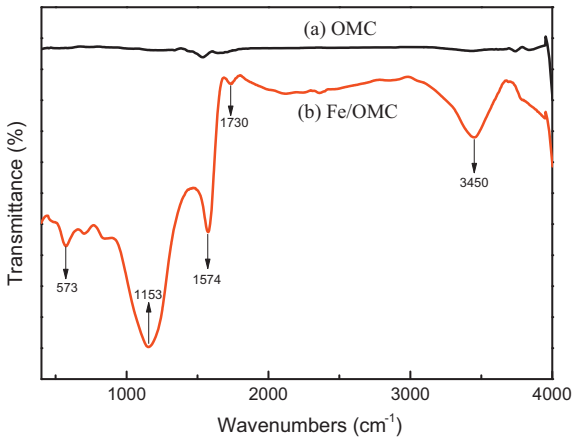

Fig. 6. FTIR spectra of OMC and Fe/OMC.

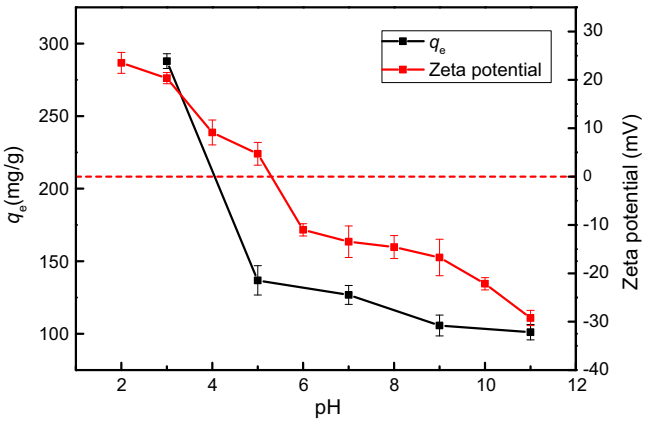

Fig. 8. Effect of pH values on adsorption of 2,4-D onto Fe/OMC at 30 °C (initial concentration, 400 mg/L).

stretching vibrations in ether groups on the surface of Fe/OMC. The characteristic peak at 573 cm^{-1} that is clearly observed in Fe/OMC spectrum is assigned to the Fe–O stretch vibration, indicating Fe_3O_4 nanoparticles were successfully doped in the OMC.

Magnetization curve of Fe/OMC is shown in Fig. 7, which exhibits near-zero coercivity and remanence, indicating a superparamagnetic nature of Fe/OMC. The saturation magnetization strength of Fe/OMC was 4.74 A m^2/kg. The magnetic separation of Fe/OMC was detected in solution by external magnetic field. The material could be completely separated within 5 min. From the above, Fe/OMC possessed a good nature of magnetic separation.

3.2. The effect of initial pH on adsorption of 2,4-D

The initial pH of solution is one of the most important factors influencing the properties of adsorbate, adsorbent and the adsorption process. The influence of initial pH was attributed to the electrostatic interaction between the 2,4-D and the Fe/OMC surface [33]. The effect of solution pH on adsorption of 2,4-D by Fe/OMC was studied in the pH range of 3–11 with initial 2,4-D concentration of 400 mg/L at 30 °C. As shown in Fig. 8, the adsorption amount of 2,4-D at equilibrium (q_e) decreased from 287.92 to 101.08 mg/g with increase of pH from 3 to 11. The maximum adsorption was obtained at pH 3. It suggested that the 2,4-D adsorption was highly dependent on solution pH. Solubility of 2,4-D in water is lower than 900 mg/L, and 2,4-D is an acidic chemical substance which is present as deprotonated form (anion) in water solution. Its solubility is even poorer in acid solution which may lead to removal of 2,4-D at high efficiency. On the other hand, the dissociation constant (pK_a) of 2,4-D is 2.64 [4], so some 2,4-D molecules are in the ionized form when the pH value of solution is higher than 2.64, and the degree of dissociation of 2,4-D increases gradually with pH increase which makes it more negatively charged. What is more, the surface charge of Fe/OMC is neutral at pH of 5.3 (pH_{PZC}), as shown in Fig. 8. It means that the Fe/OMC surface is positively charged at pH below 5.3 and negatively charged at pH above 5.3. Hence, the adsorbing capacity to 2,4-D is relatively high in acid condition than that in alkaline conditions due to the electrostatic attraction.

3.3. The effect of contact time and initial concentration on adsorption of 2,4-D

The effect of contact time on 2,4-D adsorption was investigated at pH 3 and 30 °C. As shown in Fig. 9, most of 2,4-D was rapidly absorbed on Fe/OMC within 5 min. The reason might be that 2,4-D was rapidly transported to the inside of the adsorbent by the unique hexagonal pore structure, and the strong affinity existed between 2,4-D and the carboxylate groups on the mesoporous carbon. After that, the adsorption rate of 2,4-D became low until the adsorption equilibrium was reached after 2 h. It was attributed to that the most of adsorption sites have been occupied, leading to a decline in adsorption rate. After this, the removal percentage of

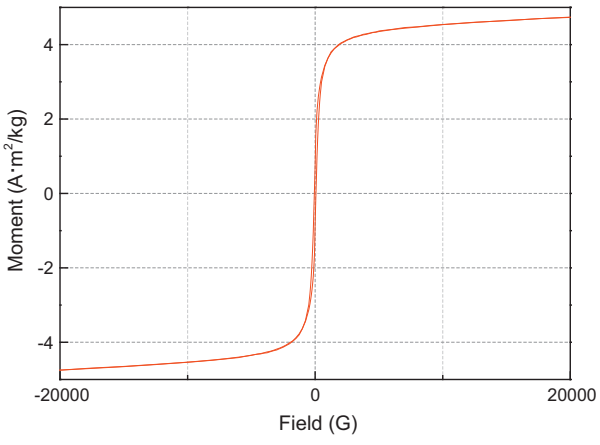

Fig. 7. Magnetization curves of Fe/OMC.

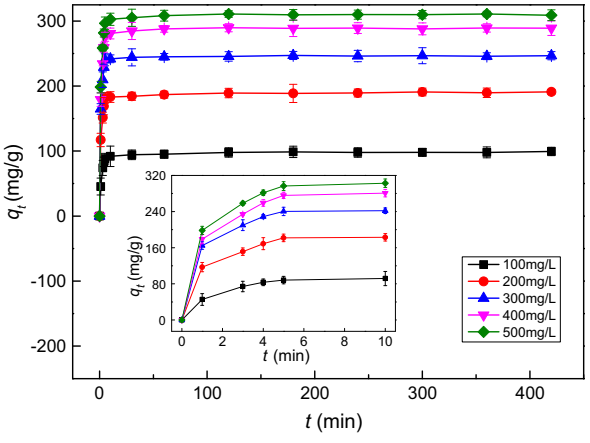

Fig. 9. Effect of contact time and initial concentration on adsorption of 2,4-D onto Fe/OMC at 30 °C (pH 3; agitation speed, 120 rpm).

2,4-D has almost no change with further increase of the contact time. At this point, the adsorption and desorption amount of 2,4-D reached the state of dynamic equilibrium.

Moreover, the amount of the adsorbed 2,4-D at equilibrium increased from 99.38 to 310.78 mg/g with the increase of the initial concentration of 2,4-D from 100 to 500 mg/L. Two possible reasons might explain this phenomenon. First, the active sites of Fe/OMC were further utilized with the increase of the concentration of 2,4-D. Second, the probability of collision between 2,4-D molecules and Fe/OMC was continually enhanced with the increase of the concentration of 2,4-D. However, the percentage of removal (R_r) decreased from 99.38% to 62% with the increase of the initial concentration of 2,4-D from 100 to 500 mg/L. This could be ascribed to that the available active sites got saturated. With the continuing increase of the initial concentration of 2,4-D, the growth rate of the adsorption amount at equilibrium declined when the saturation was approaching.

3.4. The effect of temperature on adsorption of 2,4-D

The effect of temperature toward 2,4-D adsorption was investigated at the initial 2,4-D concentration of 400 mg/L. As shown in Table 1, The adsorption capacity for 2,4-D decreased from 270.60 to 256.38 mg/g with the increase of the temperature from 30 to 50 °C. The result indicated that the process of the adsorption was exothermal. The decline of removal rate might be attributed to the solubility of 2,4-D. However, the solubility of 2,4-D in water improved continually with the increase of the temperature, which would cause more 2,4-D dissolve in water. Furthermore, as the temperature increased, the vibrational energy of 2,4-D adsorbed on the Fe/OMC surface was increased accordingly. Therefore, 2,4-D molecules would overcome the adsorptive forces and return to the solution. This could result in a lower adsorption of 2,4-D on Fe/OMC at higher temperatures.

3.5. Adsorption kinetics

The experimental data were compared to two kinetic models, the pseudo-first-order (PFO) and pseudo-second-order (PSO). The PFO model is based on the assumption that the adsorption rate is determined by the number of adsorption sites on the surface of the adsorbent; the PSO model is based on the assumption that the adsorption rate is determined by the square of the number of vacant adsorption sites on the surface of the adsorbent [34]. The formula of Lagergren's PFO kinetic model [35] is expressed by

$$q_t = q_e\left(1 - e^{-k_1 t}\right) \tag{3}$$

where k_1 (min^{-1}) is the rate constant of PFO kinetic; q_e is the amount of adsorbed 2,4-D at equilibrium. By contrast, the PSO model by Ho [36] is as follow.

$$q_t = \frac{q_e^2 k_2 t}{1 + q_e k_2 t} \tag{4}$$

where k_2 (g mg^{-1} min^{-1}) is the rate constant of PSO kinetic model. The two models were applied by nonlinear regression to fit the data of batch adsorption experiment by the OriginPro 9.0 data analysis, and the analytical result is shown in Fig. 10. The kinetic model

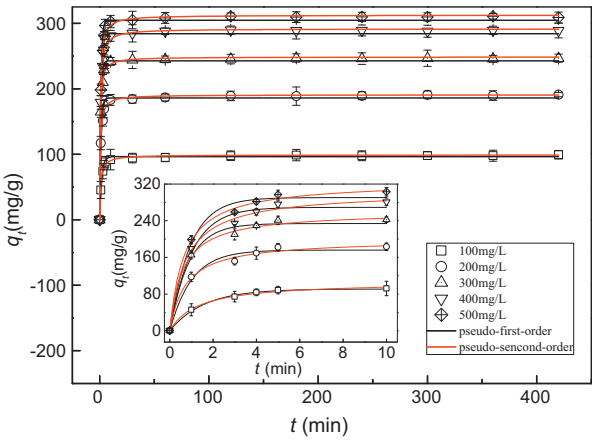

Fig. 10. Kinetic modeling for the adsorption of 2,4-D onto Fe/OMC at 30 °C (pH 3; agitation speed, 120 rpm).

parameters, adjusted correlation coefficient (R^2_{adj}) and root-mean squared error (RMSE) are shown in Table 2. It was found that the R^2_{adj} of PSO model was very close to 1. It means that the adsorption kinetics of 2,4-D on Fe/OMC was primarily elaborated by the PSO model. The lowest RMSE values further demonstrate the suitability of PSO model in describing the adsorption of 2,4-D. In addition, the uniformity between the experimental values of equilibrium adsorption capacity (q_e) and the theoretical values proved that the adsorption experiment was well fitted by the PSO model once again. The result suggested the adsorption rate was closely related to the effective number of adsorption sites of Fe/OMC rather than the concentration of 2,4-D.

3.6. Adsorption isotherms

The adsorption equilibrium data were compared to three isotherm models which illustrate the specific relationship between the solid adsorbent and the adsorbate molecules, namely the Langmuir isotherm, the Freundlich isotherm and the Temkin isotherm model. Langmuir isotherm model was established by the two hypotheses. First, adsorbent surface is homogeneous with identical adsorption sites. Second, each adsorption sites can only accommodate an adsorbate molecule. The equation of Langmuir isotherm model [37] is expressed by

$$q_e = \frac{q_m K_L C_e}{1 + K_L C_e} \tag{5}$$

where q_m (mg/g) is the maximum monolayer adsorption capacity of 2,4-D on Fe/OMC; K_L (L/mg) is free energy of adsorption process; C_e is the residual concentration of 2,4-D solution when the adsorption experiment reaches equilibrium state. Langmuir isotherm model still has an essential characteristic called separation factor (R_L), which is expressed as

$$R_L = \frac{1}{1 + K_L C_0} \tag{6}$$

the types of isotherms can be determined by the value of the separation factor as follows: irreversible ($R_L = 0$), favorable

Table 1
Adsorption capacity and thermodynamic properties for the adsorption of 2,4-D onto Fe/OMC.

Temperature (°C)	Adsorption capacity (mg/g)	K_d	$\Delta H°$ (kJ/mol)	$\Delta S°$ (J/mol K)	$\Delta G°$ (kJ/mol)
30	270.60 ± 4.64	2.09			−1.88
40	265.56 ± 6.26	1.97	−6.41	−14.97	−1.73
50	256.38 ± 10.13	1.79			−1.58

Table 2
Kinetic model parameters for adsorption of 2,4-D onto Fe/OMC at 30 °C.

C_0 (mg/L)	Pseudo-first-order				Pseudo-second-order			
	k_1 (min^{-1})	q_e (mg/g)	R^2_{adj}	RMSE	k_2 (g mg^{-1} min^{-1})	q_e (mg/g)	R^2_{adj}	RMSE
100	0.53	96.53	0.991	0.89	0.010	99.06	0.992	0.92
200	0.80	186.07	0.978	2.42	0.009	190.86	0.993	1.50
300	1.01	242.79	0.986	2.37	0.009	248.65	0.994	1.70
400	0.82	284.27	0.981	3.43	0.006	291.56	0.995	2.02
500	0.90	304.76	0.984	3.32	0.006	312.54	0.996	1.91

($0 < R_L < 1$), linear ($R_L = 1$), and unfavorable ($R_L > 1$) [37]. The Freundlich isotherm model depicts the reversible adsorption over the heterogeneous surface of adsorbent through extensive experience [38]. The equation is given as

$$q_e = K_F C_e^{\frac{1}{n}} \tag{7}$$

where n and K_F (mg/g) (L/mg)$^{1/n}$ represent Freundlich isotherm constants related to adsorption intensity and adsorption capacity, respectively. The favorability of the process was indicated by the magnitude of n, and values of $n > 1$ represent favorable adsorption. Temkin isotherm model describes the effects of adsorbate–adsorbate interactions based on the assumption that the adsorptive heat of all molecules would decrease linearly with surface coverage, and has a forecasting ability in the range of wide concentration [39]. The equation is expressed as:

$$q_e = B(\ln K_t + \ln C_e) \tag{8}$$

where K_t (L/mg) is the Temkin isotherm constant related to the maximum binding energy, $B = RT/b$ represents the adsorptive heat, R (8.314 J/mol K) is the gas constant, T (K) is the absolute temperature, and b indicates the adsorption potential of the adsorbent [40].

The adsorption data was compared to the different isotherms including the Langmuir isotherm, the Freundlich isotherm and the Temkin isotherm model by nonlinear regression method, and the results are shown in Fig. 11. The important isotherm parameters were calculated according to the three-parameter isotherm and summed up in Table 3. Through a comparison of R^2_{adj} of isotherm models, the Langmuir isotherm and the Temkin isotherm model were better. Furthermore, the RMSE of the Langmuir isotherm model was less than that of the Temkin isotherm model. So, the Langmuir isotherm model was the most appropriate to describe the correlation of the experimental data in the concentration range studied. According to Langmuir model, the maximum monolayer adsorption capacity of 2,4-D on Fe/OMC was 300.42 mg/g. The value

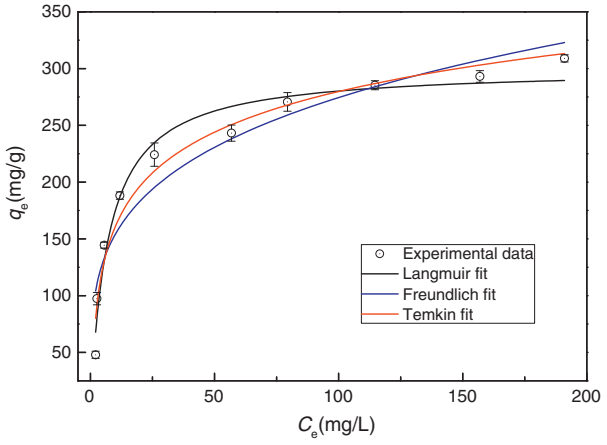

Fig. 11. Adsorption isotherm for adsorption of 2,4-D onto Fe/OMC at 30 °C (pH 3; agitation speed, 120 rpm).

of the separation factor ($0 < R_L = 0.02 < 1$) means that the adsorption process of 2,4-D was favorable. The best applicability of the Langmuir model to describe the adsorption process may be due to that the adsorption sites were evenly distributed in Fe/OMC surface.

3.7. Adsorption thermodynamics

The adsorption process of 2,4-D at different temperatures was described by three thermodynamic properties, standard enthalpy ($\Delta H°$), standard entropy ($\Delta S°$) and standard free energy ($\Delta G°$). The thermodynamic properties were calculated using the following expression:

$$\ln K_d = \frac{\Delta S°}{R} - \frac{\Delta H°}{RT} \tag{9}$$

$$K_d = \frac{C_{ad,e}}{C_e} \tag{10}$$

$$\Delta G° = \Delta H° - T\Delta S° \tag{11}$$

where K_d is the distribution coefficient; $C_{ad,e}$ (mg/L) and C_e are equilibrium concentration of 2,4-D on Fe/OMC and the equilibrium concentration of 2,4-D in solution, respectively. R and T have been defined in the above. $\Delta H°$, $\Delta S°$ can be calculated from the intercept and the slope, respectively, in linear fit of formula (9). The values of K_d, $\Delta H°$, $\Delta S°$, $\Delta G°$ are calculated and summarized in Table 1. The negative value of $\Delta H°$ demonstrates the exothermic nature of the adsorption of 2,4-D onto Fe/OMC, and its small absolute value means that the adsorption of 2,4-D was mainly a physisorption process. Similar observations were made by El Bakouri et al. [41] and Salman et al. [42]. The negative value of $\Delta S°$ indicated the decrease of randomness at the solid–solution interface and the good affinity of Fe/OMC for 2,4-D during the whole adsorption process. The negative values of $\Delta G°$ at different temperatures indicated that the adsorption process of 2,4-D onto Fe/OMC was feasible and spontaneous.

3.8. Regeneration of Fe/OMC

Due to the adsorption of 2,4-D onto Fe/OMC was a reversible process, the regeneration of the adsorbed Fe/OMC was conducted using the dipping of ethanol and magnet separation. Ethanol was commonly used an efficient desorption solvent for desorption of organic compounds, such as 2,4-D [43,44]. The Fe/OMC was repeatedly putted into 400 mg/L solution of 2,4-D for adsorption and taken out for regeneration. In each cycle, the percentage of removal (R_r) was calculated using Eq. (2) for the adsorption process. The regeneration results were shown in Fig. 12. R_r decreased obviously at the 2 and 3 cycles, but little decrease was observed with the increase of the times of cycle. The initial decrease may be due to the decreasing of carboxyl functional groups of the Fe/OMC surface by ethanol treatment. It was found in the experiment that the hydrophilicity of Fe/OMC decreased a little after desorption, probably because a few of the carboxyl groups fell off due to their strong affinity with 2,4-D in the initial desorption treatment. But finally, the adsorption efficiency could still remain high after six

Table 3
Adsorption isotherm model parameters for adsorption of 2,4-D onto Fe/OMC.

Langmuir				Freundlich				Temkin			
K_L (L/mg)	q_m (mg/g)	R^2_{adj}	RMSE	K_F (mg/g)(L/mg)$^{1/n}$	n	R^2_{adj}	RMSE	K_t (L/mg)	B	R^2_{adj}	RMSE
0.14	300.42	0.969	8.81	86.38	3.98	0.912	12.20	0.02	51.70	0.968	11.30

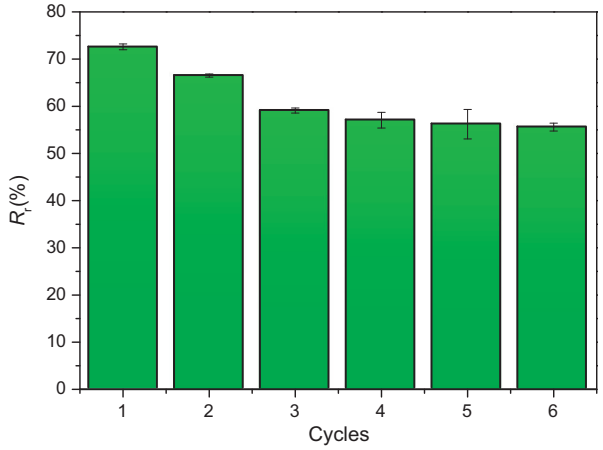

Fig. 12. Adsorption–desorption cycles of Fe/OMC for 2,4-D.

cycles as to the high initial concentration of 2,4-D, which indicated that Fe/OMC had a good capacity of regeneration and repeatability.

4. Conclusions

In this work, a mesoporous carbon functionalized with carboxylate groups and iron oxide nanoparticles was successfully synthesized and used to remove 2,4-D from wastewater. The synthesized mesoporous carbon possessed high degree of order, high specific surface area, large pore volume and good magnetic properties, exhibited large adsorption capacity at low pH and low temperature, and could be easily separated. The pseudo-second-order kinetic and Langmuir isotherm models were well fitted to the adsorption data. Furthermore, the adsorbed Fe/OMC could be regenerated by dipping into ethanol to regain its adsorption capacity. Especially, it is the most important that Fe/OMC possessed the capacity of rapid adsorption for 2,4-D. Therefore, we believe that Fe/OMC can be applied for rapid adsorption of organic pollutants from industrial effluents, and prevent further diffusion of contaminant, which can largely reduce the costing time of pollutant treatment.

Acknowledgments

The study was financially supported by the Young Top-Notch Talent Support Program of China (2012), the National Natural Science Foundation of China (51222805), the Program for New Century Excellent Talents in University from the Ministry of Education of China (NCET-11-0129), Interdisciplinary Research Project of Hunan University, the Fundamental Research Funds for the Central Universities, Hunan University, and Foundation for the Author of Excellent Doctoral Dissertation of Hunan Province.

References

[1] David H. Garabrant, Martin A. Philbert, Crit. Rev. Toxicol. 32 (2002) 233.
[2] V.O. Njoku, B.H. Hameed, Chem. Eng. J. 173 (2011) 391.
[3] M.A. Oturan, J. Appl. Electrochem. 30 (2000) 475.
[4] Z. Aksu, E. Kabasakal, Sep. Purif. Technol. 35 (2004) 223.
[5] B.H. Hameed, J.M. Salman, A.L. Ahmad, J. Hazard. Mater. 163 (2009) 121.
[6] Duygu Ova, Bikem Ovez, J. Environ. Chem. Eng. 1 (2013) 813.
[7] Lixia Yang, Wensi Sun, Shenglian Luo, Yan Luo, Appl. Catal., B 156–157 (2014) 25.
[8] Satoshi Horikoshi, Hisao Hidaka, Nick Serpone, J. Photochem. Photobiol., A 159 (2003) 289.
[9] Jing-yun Ma, Xiang-chun Quan, Zhi-feng Yang, An-jie Li, Chem. Eng. J. 181–182 (2012) 144.
[10] Ying Hua Xu, Qian Qian Cai, Hong Xing Ma, Yan He, Hong Zhang, Chun An Ma, Electrochim. Acta 96 (2013) 90.
[11] Chen Sun, Shams Ali Baig, Zimo Lou, Jin Zhu, Zhuoxing Wang, Xia Li, Jiahan Wu, Yifu Zhang, Xinhua Xu, Appl. Catal., B 158–159 (2014) 38.
[12] JingLi Zhang, ZhanPing Cao, HongWei Zhang, LianMei Zhao, XuDong Sun, Feng Mei, J. Hazard. Mater. 262 (2013) 137.
[13] Carla Badellino, Christiane Arruda Rodrigues, Rodnei Bertazzoli, J. Hazard. Mater. 137 (2006) 856.
[14] Meghdad Pirsaheb, Abdollah Dargahi, Sadegh Hazrati, Mehdi Fazlzadehdavil, Desalination Water Treat. 52 (2013) 4350.
[15] Vinod K. Gupta, Imran Ali, Suhas, Vipin K. Saini, J. Colloid Interface Sci. 299 (2006) 556.
[16] Guide Yang, Lin Tang, Xiaoxia Lei, Guangming Zeng, Ye Cai, Xue Wei, Yaoyu Zhou, Sisi Li, Yan Fang, Yi Zhang, Appl. Surf. Sci. 292 (2014) 710.
[17] Wen Li, Yankui Tang, Yutao Zeng, Zhangfa Tong, Dawen Liang, Weiwei Cui, Chem. Eng. J. 193–194 (2012) 88.
[18] G. Kyriakopoulos, D. Doulia, E. Anagnostopoulos, Chem. Eng. Sci. 60 (2005) 1177.
[19] Timothy J. Buran, Amandeep K. Sandhu, Zheng Li, Cheryl R. Rock, Weihua W. Yang, Liwei Gu, J. Food Eng. 128 (2014) 167.
[20] Lili Ding, Bo Zou, Wei Gao, Qi Liu, Zichen Wang, Yupeng Guo, Xiaofeng Wang, Yanhua Liu, Colloids Surf., A 446 (2014) 1.
[21] Allen Chaparadza, Jeanne M. Hossenlopp, J. Colloid Interface Sci. 363 (2011) 92.
[22] Milan Z. Momčilović, Marjan S. Ranđelović, Aleksandra R. Zarubica, Antonije E. Onjia, Maja Kokunešoski, Branko Z. Matović, Chem. Eng. J. 220 (2013) 276.
[23] Lin Tang, Gui-De Yang, Guang-Ming Zeng, Ye Cai, Si-Si Li, Yao-Yu Zhou, Ya Pang, Yuan-Yuan Liu, Yi Zhang, Brandon Luna, Chem. Eng. J. 239 (2014) 114.
[24] Piotr A. Bazuła, An-Hui Lu, Jörg-Joachim Nitz, Ferdi Schüth, Microporous Mesoporous Mater. 108 (2008) 266.
[25] Lin Tang, Yan Fang, Ya Pang, Guangming Zeng, Jiajia Wang, Yaoyu Zhou, Yaocheng Deng, Guide Yang, Ye Cai, Jun Chen, Chem. Eng. J. 254 (2014) 302.
[26] Yuanyuan Liu, Zhuotong Zeng, Guangming Zeng, Lin Tang, Ya Pang, Zhen Li, Can Liu, Xiaoxia Lei, Mengshi Wu, Pinyun Ren, Zhifeng Liu, Ming Chen, Gengxin Xie, Bioresour. Technol. 115 (2012) 21.
[27] Lin Tang, Ye Cai, Guide Yang, Yuanyuan Liu, Guangming Zeng, Yaoyu Zhou, Sisi Li, Jiajia Wang, Sheng Zhang, Yan Fang, Yibin He, Appl. Surf. Sci. 314 (2014) 746.
[28] Zhangxiong Wu, Paul A. Webley, Dongyuan Zhao, Langmuir: ACS J. Surf. Colloids 26 (2010) 10277.
[29] Yue Chi, Wangchang Geng, Liang Zhao, Xiao Yan, Qing Yuana, Nan Li, Xiaotian Li, J. Colloid Interface Sci. 369 (2012) 366.
[30] Dongyuan Zhao, Qisheng Huo, Jianglin Feng, Bradley F. Chmelka, Galen D. Stucky, J. Am. Chem. Soc. 120 (1998) 6024.
[31] Shinae Jun, Sang Hoon Joo, Ryong Ryoo, Michal Kruk, Mietek Jaroniec, Zheng Liu, Tetsu Ohsuna, Osamu Terasaki, J. Am. Chem. Soc. 122 (2000) 10712.
[32] M.J. Lázaro, L. Calvillo, E.G. Bordejé, R. Moliner, R. Juan, C.R. Ruiz, Microporous Mesoporous Mater. 103 (2007) 158.
[33] V.O. Njoku, K.Y. Foo, B.H. Hameed, Chem. Eng. J. 215–216 (2013) 383.
[34] Asma Turki, Chantal Guillard, Frédéric Dappozze, Zouhaier Ksibi, Gilles Berhault, Hafedh Kochkar, Appl. Catal., B 163 (2015) 404.
[35] Stan Lagergren, Veternskapsakad Handlingar 24 (1898) 1.
[36] Y.S. Ho, G. McKay, Process Biochem. 34 (1999) 451.
[37] Milan Z. Momčilović, Antonije E. Onjia, Milovan M. Purenović, Aleksandra R. Zarubica, Marjan S. Ranđelović, J. Serb. Chem. Soc. 77 (2012) 761.
[38] Herb Freundlich, Z. Phys. Chem. 57 (1906) 384.
[39] M.I. Temkin, V. Pyzhev, Acta Physiochim. URSS 12 (1940) 217.
[40] Milan Momčilović, Milovan Purenović, Aleksandar Bojić, Aleksandra Zarubica, Marjan Ranđelović, Desalination 276 (2011) 53.
[41] Hicham El Bakouri, José Usero, José Morillo, Abdelhamid Ouassini, Bioresour. Technol. 100 (2009) 4147.
[42] J.M. Salman, V.O. Njoku, B.H. Hameed, Chem. Eng. J. 174 (2011) 33.
[43] J.M. Salman, B.H. Hameed, J. Hazard. Mater. 176 (2010) 814.
[44] Beom K. Jung, Zubair Hasan, Sung Hwa Jhung, Chem. Eng. J. 234 (2013) 99.